

**The microstructural and metamorphic history  
preserved within garnet porphyroblasts  
from southern Vermont and northwestern Massachusetts**

**VOLUME II**

Thesis submitted by

Bronwyn Patricia GAVIN BSc (Hons) *Canterbury, NZ*

in June 2004

for the degree of Doctor of Philosophy

in the School of Earth Sciences

James Cook University

## **SECTION A**

---

**The orientation of textural discontinuities in garnets with  
complex spiral inclusion trails**

---

### List of Tables and Figures

Table A-1: Trend and plunge of Foliation Intersection/Inflection Axes (FIAs) for selected samples.	A-3
Figure A-1: Diagram showing how curved inclusion trails can be produced without porphyroblast rotation.	A-4
Figure A-2: Diagram showing how orthogonal foliations can be produced.	A-5
Figure A-3: Diagram showing examples of textural discontinuities.	A-7
Figure A-4: Diagram showing how textural discontinuities can form in a rotating porphyroblast and a non-rotating porphyroblast.	A-8
Figure A-5: Diagram of a rhombododecahedron, a common garnet crystal form.	A-9
Figure A-6: Map showing the location of samples mentioned in the text.	A-10
Figure A-7: Equal area rose diagrams showing the pitch of discontinuities.	A-11

Table A-1: Trend and plunge of Foliation Intersection/Inflection Axes (FIAs) for selected samples. For samples with more than one FIA the trend and plunge shown are for the core FIA.

<b>Sample</b>	<b>Trend</b>	<b>Plunge</b>
BG7	065	25
BG19	095	15
BG33	045	15
BG46	215	15
BG48	175	15
BG50	160	25
BG59	075	25
BG94	035	15
BG102B	165	45

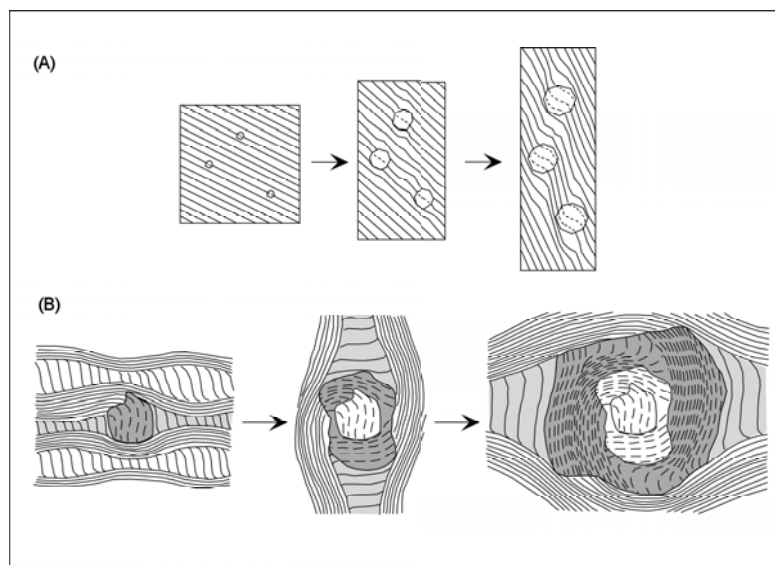


Figure A-1: Diagram showing how curved inclusion trails can be produced without porphyroblast rotation.

A: Progressive flattening with simultaneous growth of porphyroblasts can produce curved inclusion trails with up to  $90^\circ$  of apparent rotation. Differential flattening around porphyroblasts results in curvature of the surrounding schistosity and as the crystals increase in size they preserve the curved foliation as sigmoidal inclusion trails (after Ramsay, 1962).

B: Spiral inclusion trails with more than  $90^\circ$  apparent rotation can be produced by the episodic overgrowth of successive foliations. In this example, based on a real garnet porphyroblast, the first stage of growth occurs in the crenulation hinge of a horizontal foliation. Inclusion trails curve smoothly into matrix where protected by garnet edge (top left), while others are truncated (bottom edge). The second stage of garnet growth occurs in the crenulation hinge of a vertical foliation and the third stage of garnet growth in crenulation hinge of a horizontal foliation, creating a complex spiral inclusion trail with  $270^\circ$  of apparent rotation. (Modified from Bell et al., 1992, Figure 6)

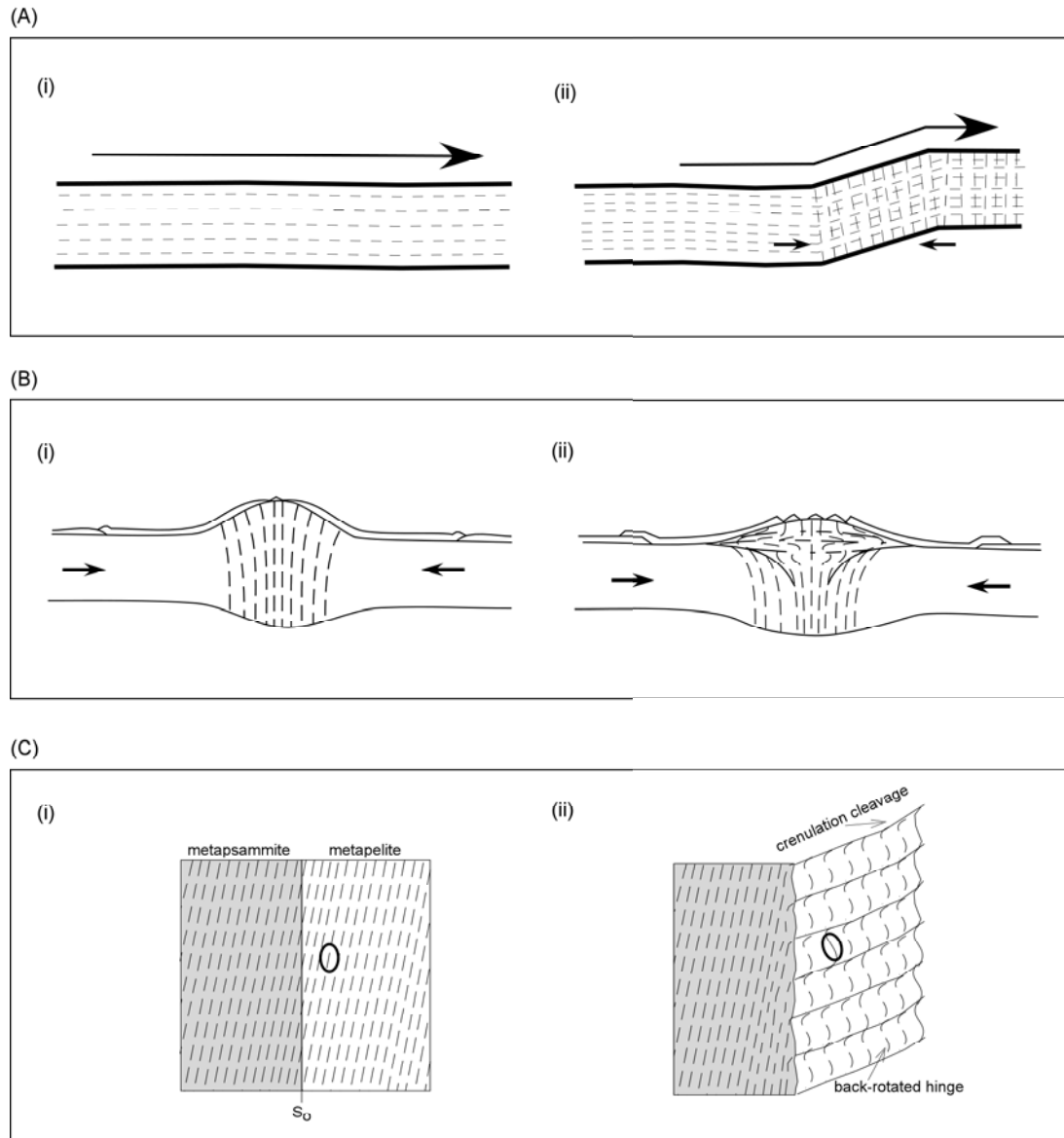


Figure A-2: Diagram showing how orthogonal foliations can be produced.

A: Production of orthogonal foliations by the passage of thrust sheets over flats and ramps.

(i) A gently dipping foliation forms when thrusting occurs across a nearly horizontal surface.

(ii) A steeply dipping foliation forms when the rocks move over a ramp and undergo layer-parallel shortening.

B: Production of orthogonal foliations by orogenic collapse (Modified from Bell and Johnson, 1989, figure 24).

(i) Crustal compression causes horizontal shortening and vertical thickening of the crust associated with a steeply dipping foliation. This causes gravitational sliding off the crown and extension in the uppermost levels.

(ii) Collapse of the over-thickened crust and gravitational spreading due to gravitational instability of the thickened pile. Localised zones of high shear strain form within the collapsing pile producing horizontal foliations.

C: Production of orthogonal foliations by back-rotation of crenulation hinges (Modified from Johnson 1999, figure 8).

(i) A porphyroblast overgrows an early foliation, preserving it as inclusion trails.

(ii) During crenulation cleavage development there is 'back-rotation' of the crenulation hinges, relative to the crenulation limbs, and the crenulation hinges eventually become orthogonal to the developing cleavage seams. The porphyroblast rotates with the crenulation hinges so that the porphyroblast inclusion trails also end-up orthogonal to the crenulation cleavage.

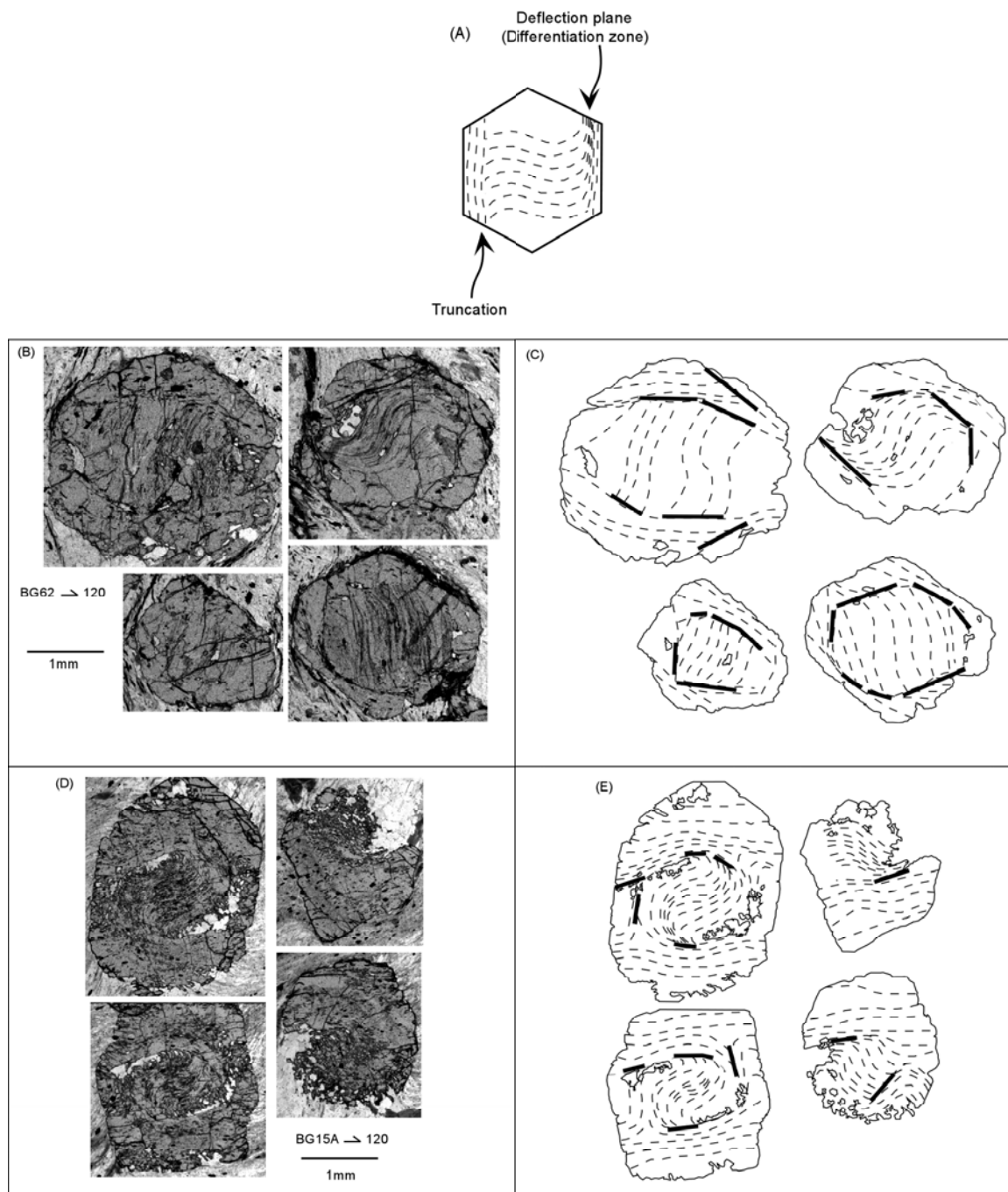


Figure A-3: Diagram showing examples of textural discontinuities.

A: Sketch of a garnet porphyroblast to illustrate the two main types of textural discontinuity.

B: Photomicrographs of garnet porphyroblasts from one vertical thin-section from sample BG62.

C: Interpretive line drawings showing inclusion trails (dashed lines) and textural discontinuities (bold lines) for the porphyroblasts from sample BG62.

D: Photomicrographs of garnet porphyroblasts from one vertical thin-section from sample BG15A.

E: Interpretive line drawings showing inclusion trails (dashed lines) and textural discontinuities (bold lines) for the porphyroblasts from sample BG15A.



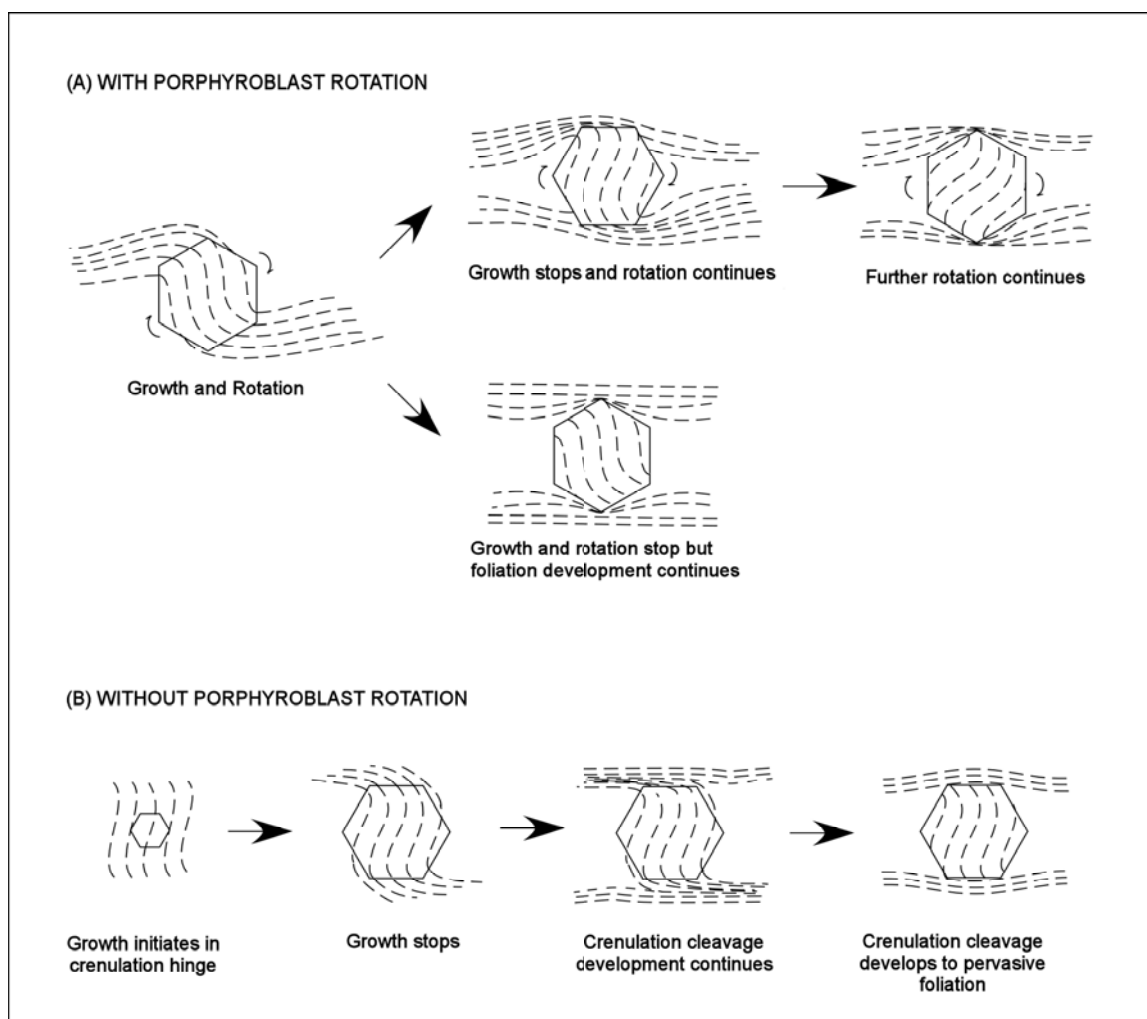


Figure A-4: Diagram showing how textural discontinuities can form in a rotating porphyroblast and a non-rotating porphyroblast (After Johnson, 1993).

A: Initial porphyroblast growth and rotation creates a smoothly curving inclusion trail then growth stops. If rotation continues zones of sharp curvature, and ultimately truncations, form between the inclusion trails and the external foliation. If rotation stops at the same time growth stops continued deformation and foliation development might create sharp truncations between the inclusion trails and the external foliation.

B: Garnet growth initiates when crenulation cleavage development begins. The porphyroblast grows in a crenulation hinge and includes the curved foliation. At a certain point porphyroblast growth stops because the porphyroblast is unable to grow out over the crenulation limb where active shearing and dissolution is taking place. Continued crenulation cleavage development results in a zone of differentiation between the inclusion trails and the external foliation. Further crenulation cleavage development results in a pervasive foliation that wraps around the porphyroblast and truncates the inclusion trails. In all cases further porphyroblast growth is needed to preserve the textural discontinuity.

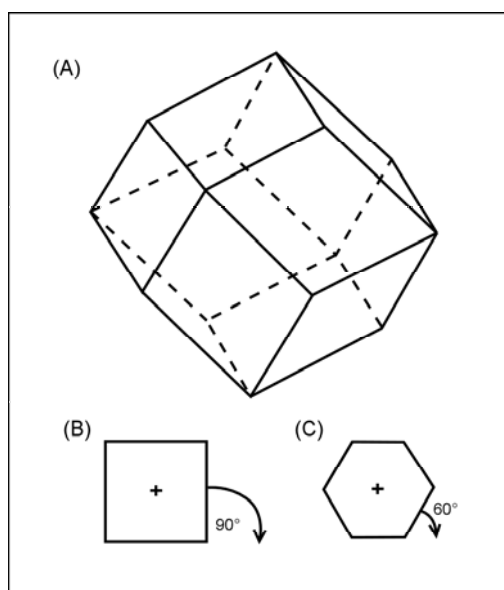


Figure A-5: Diagram of a rhombododecahedron, a common garnet crystal form.

A: A perfect rhombododecahedron has 12 identical rhombic faces and a dihedral angle of  $120^\circ$ . Like a cube it has three fourfold axes of symmetry, four threefold axes, and six twofold axes.

B: When viewed along a fourfold axis of symmetry the rhombododecahedron appears square in profile. If the crystal were rotated around this axis it would rotate in  $90^\circ$  increments.

C: When viewed along a threefold axis of symmetry the rhombododecahedron appears hexagonal in profile. If the crystal were rotated around this axis it would rotate in  $60^\circ$  increments.

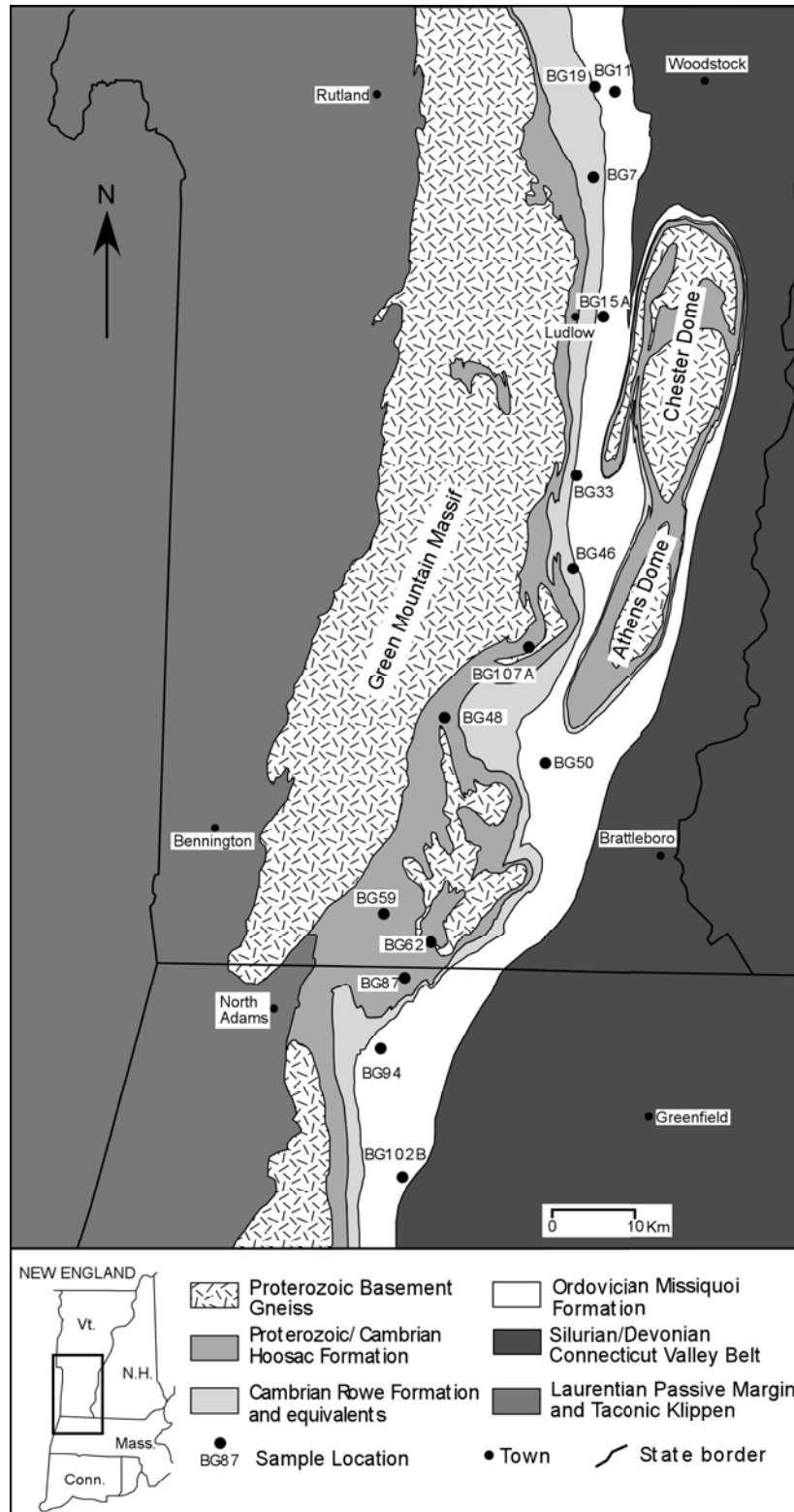


Figure A-6: Map showing the location of samples mentioned in the text. Regional geology based on Doll et al. (1961) and Zen et al. (1983).

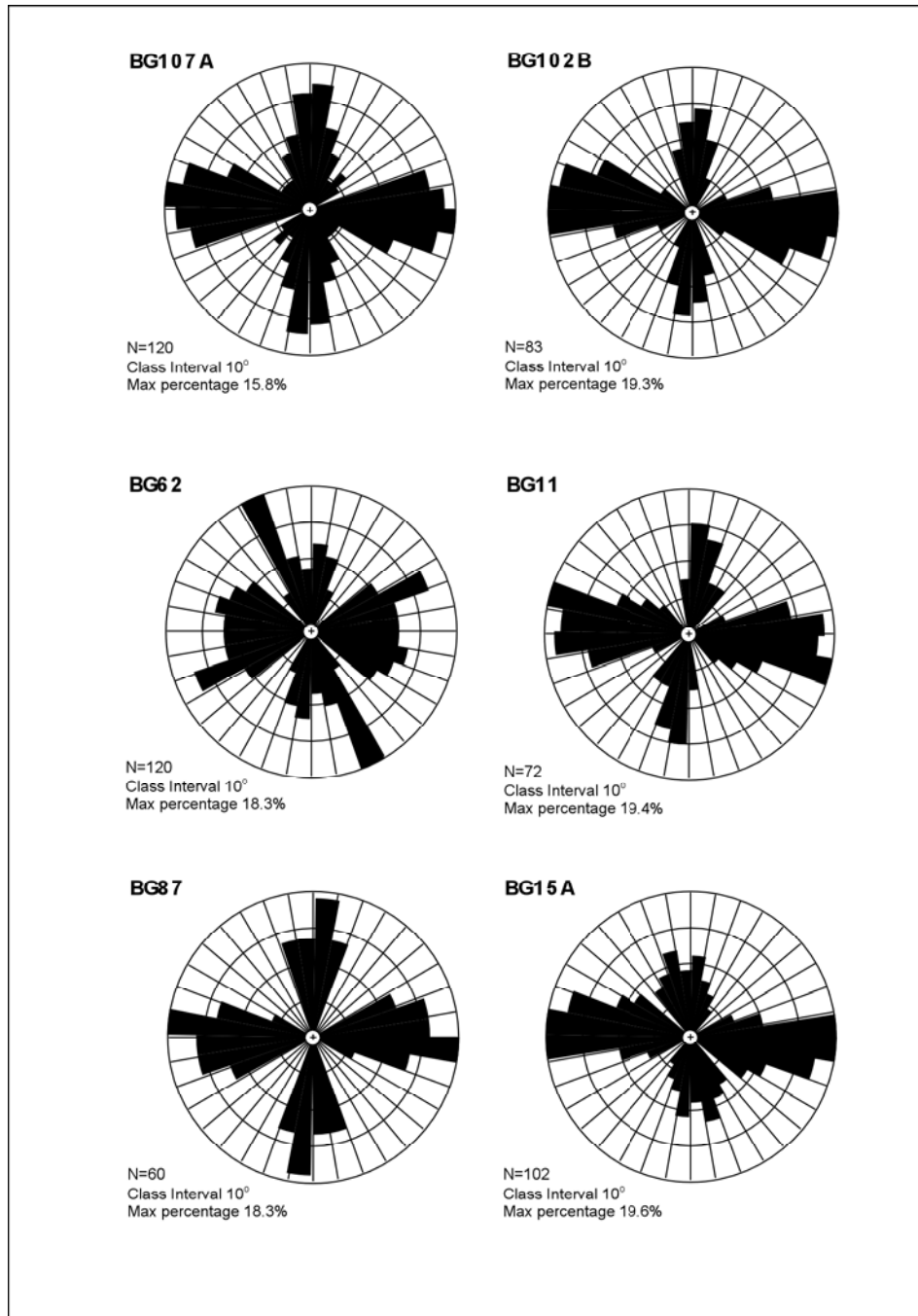


Figure A-7: Equal area rose diagrams showing the pitch of discontinuities. Zero is horizontal and 90 degrees is vertical. For each sample measurements were made from between 8 and 12 vertical thin-sections with different strikes.

## **SECTION B**

---

**Foliation Intersection/Inflection Axes in garnet  
porphyroblasts and the relationship between garnet growth  
and deformation**

---

### List of Tables and Figures

Table B-1: FIA orientation and allocated FIA set for each sample.	B-3
Table B-2: FIA orientations and allocated FIA sets for multi-FIA samples of Bell and Hickey (1997) and Bell et al. (1998).	B-4
Figure B-1: Map showing the location of samples.	B-5
Figure B-2: Equal-area rose diagrams showing total FIA data from southern Vermont and north-western Massachusetts.	B-6
Figure B-3: Diagram showing the sequence of FIAs preserved from the core to rim in multi-FIA samples.	B-7
Figure B-4: Rose diagrams and maps showing the spatial distribution of FIA sets.	B-8

Table B-1: FIA orientation and allocated FIA set for each sample. For multi-FIA samples the core FIA is listed first, followed by the median FIA (if present) and the rim FIA.

(a) Single FIA data

Sample Number	FIA Orientation	Continuous with matrix	FIA Set	Sample Number	FIA Orientation	Continuous with matrix	FIA Set
BG3	145	No	3	BG50	160	No	3
BG4	005	Yes	3.5	BG51	155	Yes	3
BG6	165	Yes	3	BG52	025	Yes	4
BG7	065	Yes	2	BG53	015	No	3.5
BG8	160	No	3	BG54	175	No	3.5
BG9	015	Yes	3.5	BG55	015	No	3.5
BG11	165	Yes	3	BG56	035	Yes	4
BG13	015	Yes	3.5	BG57B	175	No	3.5
BG14	155	Yes	3	BG58B	035	No	1
BG17	045	Yes	4	BG59	075	No	2
BG19	095	Yes	2	BG66B	145	No	3
BG20	025	Yes	4	BG69	015	Yes	3.5
BG24	155	Yes	3	BG70	075	Yes	2
BG30	175	Yes	3.5	BG71	175	Yes	3.5
BG33	045	Yes	4	BG72	030	No	1
BG35	155	Yes	3	BG78	025	Yes	4
BG38	025	Yes	4	BG80	155	No	3
BG40	175	Yes	3.5	BG81	175	Yes	3.5
BG41A	175	Yes	3.5	BG83	155	No	3
BG42	105	No	2	BG84A	045	Yes	4
BG43	075	Yes	2	BG85	175	Yes	3.5
BG44	145	Yes	3	BG86	005	Yes	3.5
BG45	160	Yes	3	BG88	075	Yes	2
BG46	035	Yes	4	BG94	035	Yes	4
BG47	025	Yes	4	BG102B	165	Yes	3
BG48	175	No	3.5	BG107A	140	No	3
BG49	155	Yes	3				

(b) Multi FIA data

Sample Number	FIA Orientations	Continuous with matrix	FIA Sets
BG15A	070 - 010	Yes	2 - 3.5
BG21	125 - 155	Yes	0 - 3
BG32	065 - 180	Yes	2 - 3.5
BG60	015 - 045	Yes	3.5 - 4
BG62	005 - 045	Yes	3.5 - 4
BG87	050 - 030	Yes	1 - 4
BG104	145 - 175	No	3 - 3.5
BG105A	145 - 175	Yes	3 - 3.5
BG108	090 - 145 - 175	No	2 - 3 - 3.5

Table B-2: FIA orientations and allocated FIA sets for multi-FIA samples of Bell and Hickey (1997) and Bell et al. (1998). Data is from Bell et al. (1998) Table 3 and Table 8. The core FIA is listed first, followed by the median FIA (if present) and the rim FIA.

Sample Number	FIA Orientations	FIA Sets	Sample Number	FIA Orientations	FIA Sets
v200A	161-011	3 - 4	v438	167 - 017	3 - 4
v209	031 - 096	1 - 2	v447A	101 - 011	2 - 4
v212E	046 - 021	1 - 4	v447B	156 - 161 - 176	3 - 3 - 3
v213	111 - 011	2 - 4	v3	016 - 161	1 - 3
v214	091 - 176	2 - 3	v17A	091 - 156	2 - 3
v443C	091 - 001	2 - 4	v300A	086 - 016	2 - 4
v444B	061 - 086	1 - 2	v334	156 - 171	3 - 3
v450A	165 - 009	3 - 4	v338A	166 - 011	3 - 4
v450B	176 - 001 - 011	3 - 4 - 4	v375B	161 - 006	3 - 4
v203	171 - 001 - 011	3 - 4 - 4	v384A	086 - 016	2 - 4
v257	036 - 166	1 - 3	v384B	081 - 016	2 - 4
v261A	026 - 161	1 - 3	v396	176 - 021 - 036	3 - 4
v261C	041 - 141	1 - 3	v413A	146 - 156	3 - 3
v360	071 - 171 - 016	2 - 3 - 4	v453A	151 - 021	3 - 4
v436A	156 - 001 - 011	3 - 4 - 4	v458A	086 - 146	2 - 3
v436D	101 - 151	2 - 3			



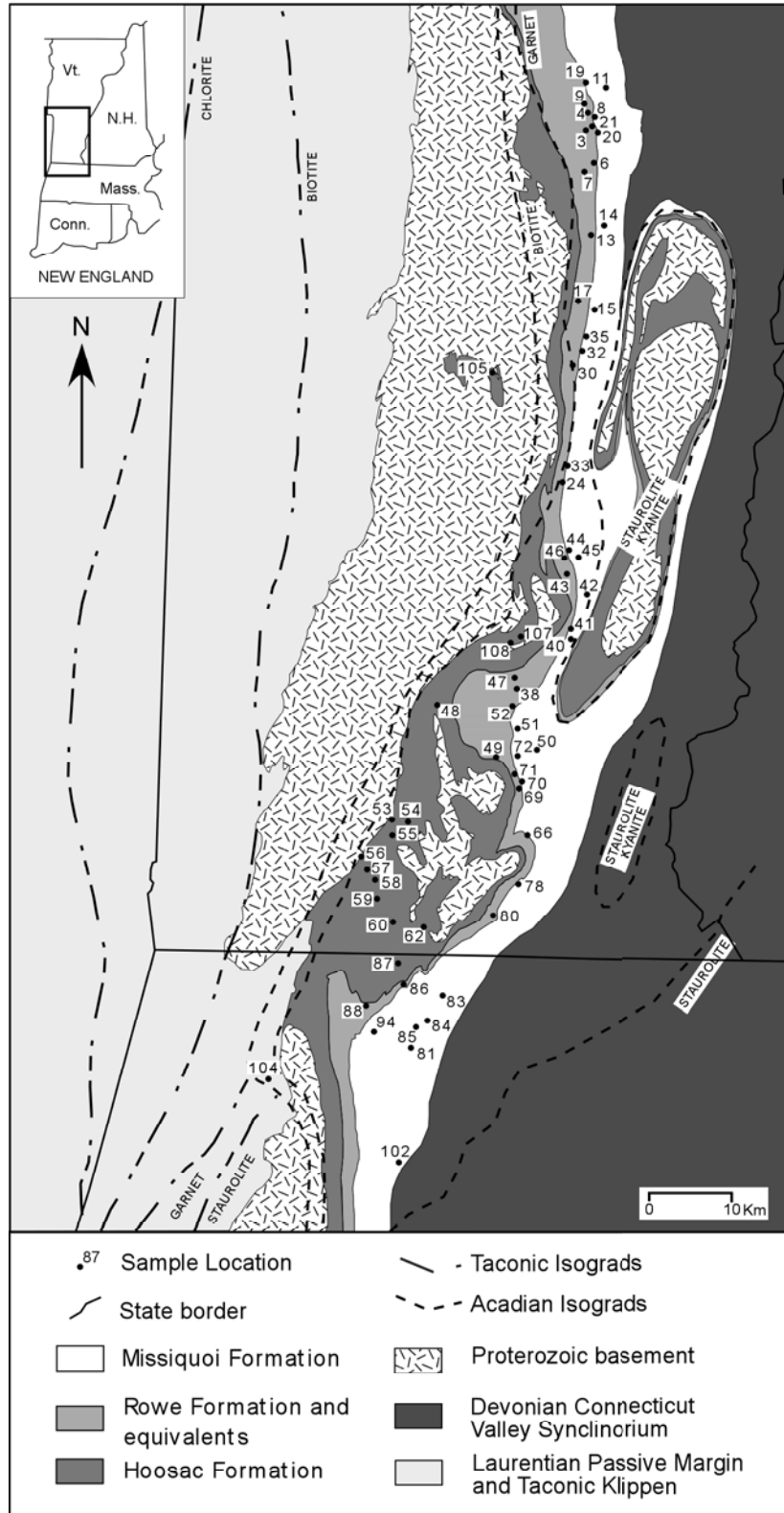


Figure B-1: Map showing the location of samples mentioned in the text. Regional geology based on Doll et al. (1961) and Zen et al. (1983). Taconic and Acadian isograds after Sutter et al. (1985).

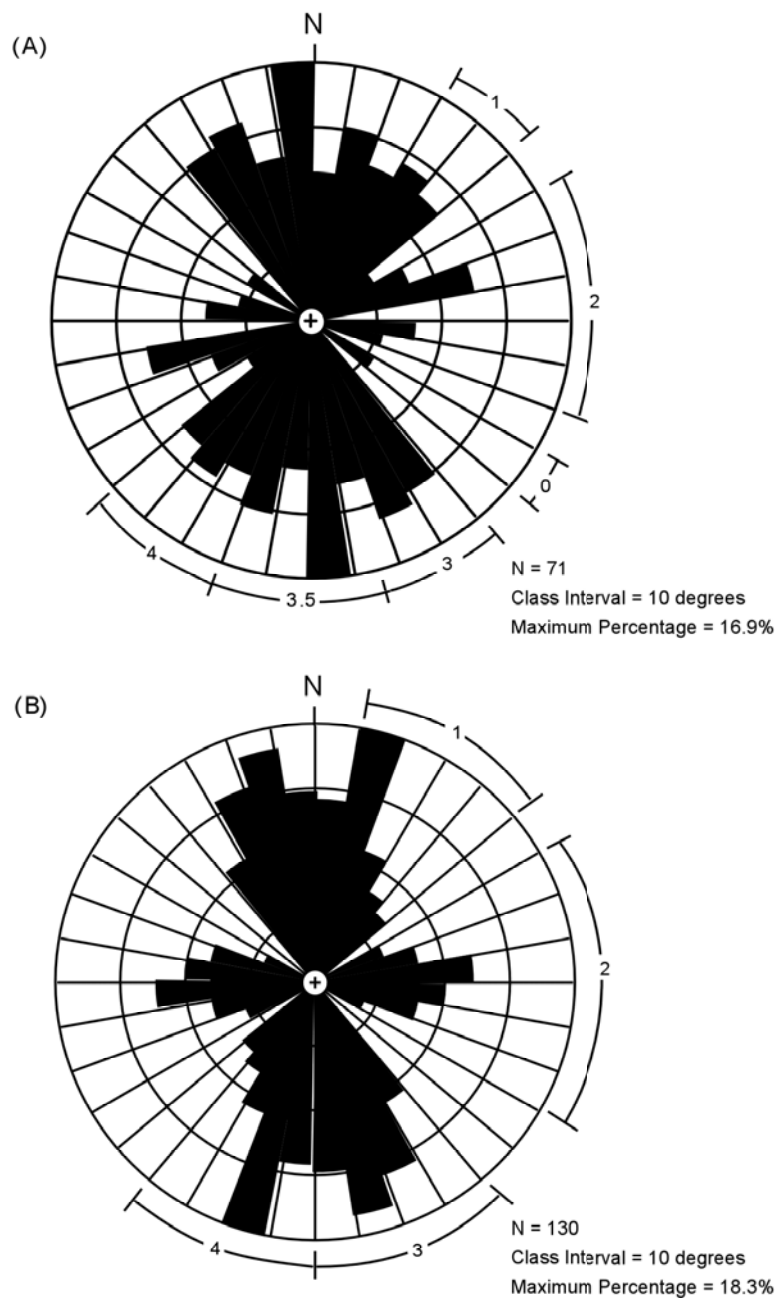


Figure B-2: Equal-area rose diagrams showing total FIA data from southern Vermont and north-western Massachusetts. The boundaries of the FIA sets are shown around the outside of the diagrams.

A: Data from this study.

B: Data from Bell et al. (1998).

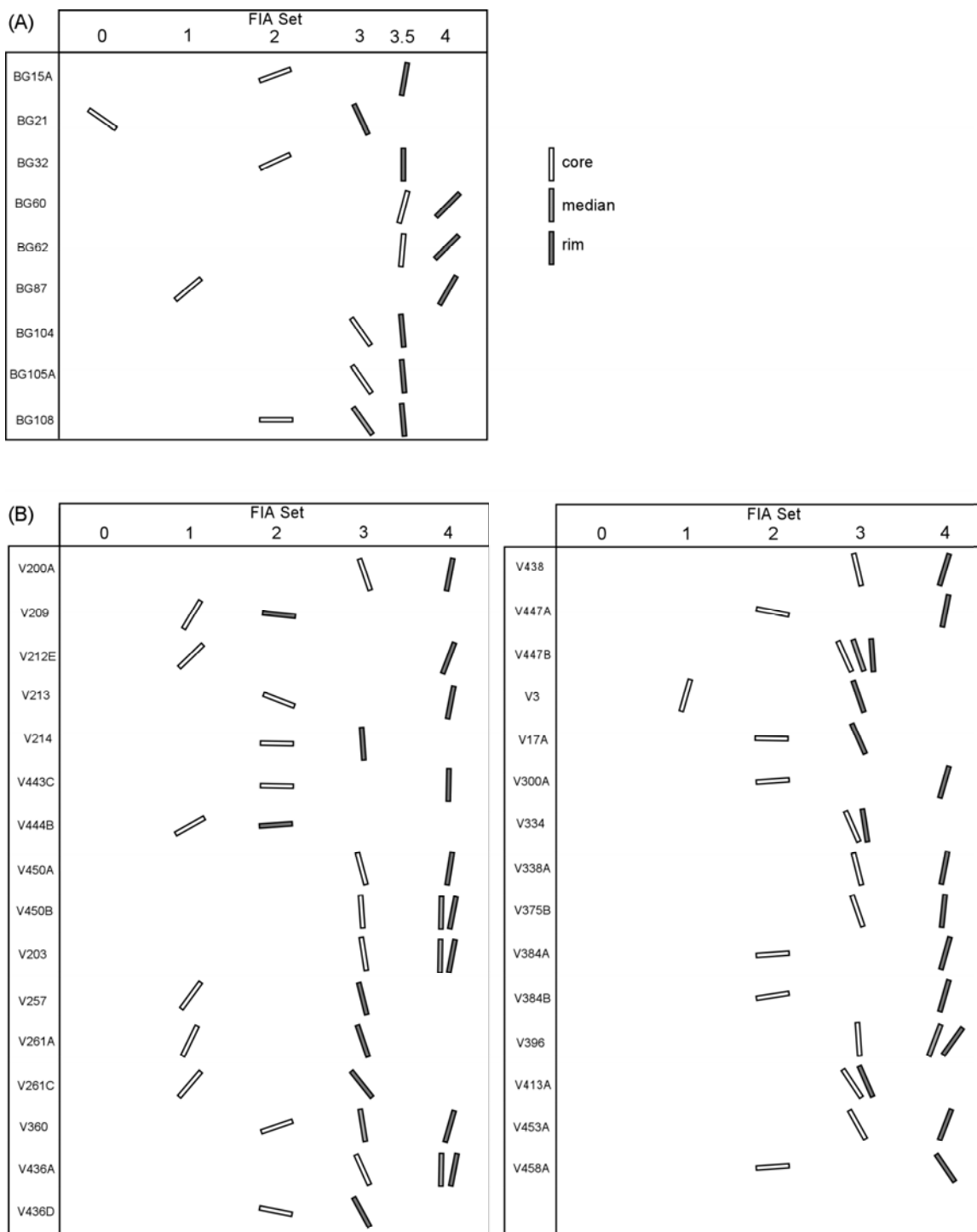


Figure B-3: Diagram showing the sequence of FIAs preserved from the core to rim in multi-FIA samples.

A: Data from this study.

B: Data from Bell et al. (1998).

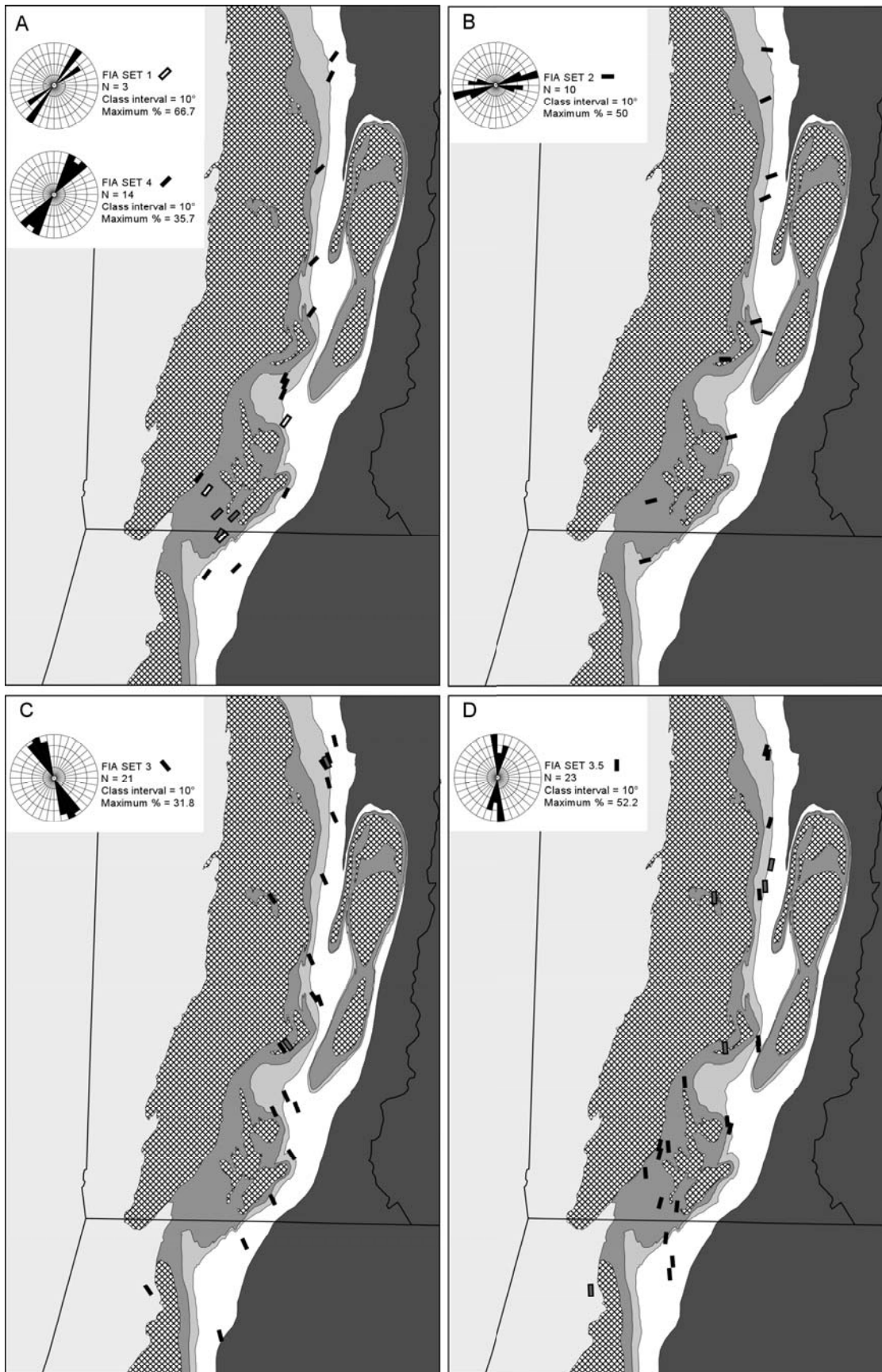


Figure B-4: Rose diagrams and maps showing the spatial distribution of FIA sets 1-4. For each sample the orientation of the rectangle indicates the orientation of the core FIA from that location. Where there has been more than one phase of growth the core growth is indicated by a black rectangle, or a white rectangle with a black border, and the median and/or rim growth is indicated by a dark grey rectangle. For geological unit names and sample numbers refer to Figure B-1.

A: FIA sets 1 (white rectangles with black border) and 4 (black rectangles).

B: FIA set 2

C: FIA set 3

D: FIA set 3.5